Cement and Concrete Research 180 (2024) 107509

Contents lists available at ScienceDirect

Cement and Concrete Research

journal homepage: www.elsevier.com/locate/cemconres

Uptake of chloride and isosaccharinic acid by cement paste with high slag content (CEM III/C)

Yongheum Jo [a,*,1], Barbara Lothenbach [b], Neşe Çevirim-Papaioannou [a], Benny de Blochouse [c], Marcus Altmaier [a], Xavier Gaona [a,**]

[a] Institute for Nuclear Waste Disposal, Karlsruhe Institute of Technology, Karlsruhe, Germany
[b] Laboratory Concrete & Asphalt, Empa, Swiss Federal Laboratories for Materials Science and Technology, Dübendorf, Switzerland
[c] ONDRAF/NIRAS, Belgian Agency for Radioactive Waste and Enriched Fissile Materials, Brussels, Belgium

ARTICLE INFO

Keywords:
Sorption
Chloride
Isosaccharinic acid (ISA)
Cement paste
High slag content

ABSTRACT

The uptake of chloride (Cl^-) and isosaccharinic acid (ISA, main degradation product of cellulose) by cement paste with high slag content (CEM III/C) was investigated with batch sorption experiments with ^{36}Cl and inactive ISA. A weak uptake of chloride was quantified ($0.43 \leq R_d$ [L•kg^{-1}] ≤ 5.8), consistently with previous observations for Portland cement. C-S-H, AFm and hydrotalcite are suggested as primary sinks for Cl^-. XRD confirmed the formation of Friedel's salt at [NaCl] $\geq$ 1 M, consistent with thermodynamic calculations. ISA exhibited moderate sorption ($9 \leq R_d$ [L•kg^{-1}] ≤ 900), successfully modeled with a one-site Langmuir isotherm. Sorption data supports that (surface) precipitation occurs at higher ISA concentrations. The formation of stable Ca-ISA aqueous complexes promotes the incongruent dissolution of cement phases, altering of the overall Ca:Si ratio. The interplay between sorption and solubility phenomena must be considered for a correct interpretation of cement-ISA systems.

1. Introduction

Cementitious materials are extensively used in repositories for low- and intermediate-level waste (L/ILW), serving not only as backfill and for construction purposes, but also for waste conditioning and stabilization [1–3]. Cement-based materials exhibit excellent capabilities for the retention of radionuclides and other contaminants due to their high sorption capacity [2,4]. Several hydrated phases dominate the composition of hydrated cement, e.g., calcium silicate hydrate (C-S-H) phases, portlandite ($Ca(OH)_2$), AFt (aluminoferrite trisulfate, with a general formula $[Ca_3(Al,Fe)(OH)_6{\cdot}12H_2O]X_3{\cdot}nH_2O$; X = M^{2+} or 2 M^+), AFm (aluminoferrite monosulfate, with a general formula of $[Ca_2(Al,Fe)(OH)_6]X{\cdot}nH_2O$), hydrogarnet ($3CaO{\cdot}Al_2O_3{\cdot}6H_2O$) or hydrotalcite (LDH, layered double hydroxide with a general formula of $Mg_6Al_2(CO_3)(OH)_{16}{\cdot}4H_2O$). C-S-H phases constitute, in most cement formulations, the major component in hydrated cement. C-S-H phases are characterized by a high surface area, and have been described to efficiently sorb cationic and (to less extent) anionic species [2]. AFm and AFt phases are able to efficiently exchange anions present in their structure, and thus are acknowledged as important sink of anionic radionuclides as well as organic ligands [5–8].

Portland cement (PC) is replaced by supplementary cementitious materials, such as fly ash and blast furnace slag, to prevent delayed ettringite formation of cemented waste drum [9] and to improve compatibility with clay materials within repository system [10]. High replacement of PC by blast furnace slag as in the case of the CEM III/C cement studied here, can result in lower pH values [11] and in the absence of portlandite [12].

Chlorine-36 (^{36}Cl, $t_{1/2} = 3.01{\cdot}10^5$ a) is a long-lived beta-emitting activation product produced through the neutron irradiation of stable ^{35}Cl (ca. 76 % natural abundance) present in fuel assemblies and structural components during operation of nuclear reactors. Wastes containing ^{36}Cl from the dismantling of nuclear reactors and the treatment of nuclear coolant are disposed in repositories for L/ILW [13–15]. In PC, C-S-H and AFm are considered as primary sinks for Cl^- rather than other phases such as portlandite and AFt [2]. The uptake mechanisms

* Correspondence to: Y. Jo, Department of Nuclear Engineering, Hanyang University, Seoul, Republic of Korea.
** Corresponding author.
E-mail addresses: yongheumjo@hanyang.ac.kr (Y. Jo), xavier.gaona@kit.edu (X. Gaona).
[1] Department of Nuclear Engineering, Hanyang University, Seoul, Republic of Korea.

https://doi.org/10.1016/j.cemconres.2024.107509
Received 19 January 2024; Received in revised form 2 April 2024; Accepted 5 April 2024
Available online 16 April 2024

include sorption on C-S-H phases, isotopic exchange with stable Cl^- present in pristine cement, and the formation of Friedel's salt ($[Ca_2(Al,Fe)(OH)_6]Cl{\cdot}2H_2O$) [2,4]. In CEM III/C cements containing a high fraction of blast furnace slag (84 [16] – 88 [17] wt%, ca. 6 wt% clinker [17]), significant amounts of hydrotalcite might form. Hydrotalcite can also play an important role in chloride binding [18–21], however mainly in the absence of carbonates [22]. The impact of portlandite and AFt, which are suppressed in CEM III/C with high slag content, on Cl^- sorption has not been accentuated [2].

The concentration of chloride in the aqueous phase is the main factor governing Cl^- sorption capacity of hydrated cement, and the fraction of chloride in solution increases with increasing $[Cl^-]$ [2,23]. Other anions such as OH^- can also influence the uptake Cl^- by competing for the sorption / ion exchange sites. Tritthart found the reduction in Cl^- binding by PC with increasing pH [24]. Hemsted et al. reported the increase of Cl^- binding by PC following the decrease in pH from 13 to 12, which was attributed to the enhanced binding capacity of AFm [25]. Jain et al. showed that Cl^- binding by cement paste at pH 11.6 and 12.6 was correlated with the release of OH^- from the cement to the pore solution, thus hinting towards the exchange of OH^- by Cl^- [26]. Surface Ca^{2+} on C-S-H plays a critical role in the adsorption of Cl^- on C-S-H by providing positively charged sorption sites and/or bridging for Cl^- surface adsorption [23,27–29].

Contaminated cotton, wood, and wipes containing cellulose can be disposed in repositories for L/ILW. Isosaccharinic acid (ISA, $C_6H_{12}O_6$) is generated under cementitious condition as a primary degradation product of cellulose [30–32]. The formation of stable complexes of ISA with several radionuclides has triggered extensive investigations on the impact of ISA on the migration of radionuclides in the context of nuclear waste disposal [33–46]. As monocarboxylic polyhydroxo ligand, ISA acts as a chelate strongly interacting with cationic radionuclides including actinides (e.g., Th(IV), U(IV/VI), Np(IV), Pu(III/IV), Am(III)), fission and activation products (e.g., Ni(II), Zr(IV)) [35–41,46]. The formation of stable complexes with ISA may result in enhanced radionuclide solubility and decreased retention properties [33,42–45]. The impact of ISA on radionuclide mobility is largely affected by the availability of free ligand in the aqueous phase. Upper concentration limits of ISA are defined by the solubility of $Ca(ISA)_2(s)$, which plays a role particularly in the degradation stage II characterized by high Ca concentrations in the pore solution. Sorption of ISA on hydrated cement is also expected to decrease the ligand concentration in the aqueous phase, especially under repository conditions where high solid-to-liquid ratios are expected. A moderate ISA uptake by hydrated cement (types CEM I and V, according to EN 197–1 [47]) has been reported at pH > 12, with R_d values ranging from ≈ 1 to ≈ 700 $L{\cdot}kg^{-1}$ depending among others on the ISA concentration in solution [23,30,42,44,48–51]. C-S-H was identified as the main hydrated cement phase sorbing ISA, but the role of other phases such as AFm and hydrotalcite involving ion exchange processes with anions cannot be ignored. For C-S-H phases, Ca was shown to play a key role in the retention process, acting as bridge between ISA and the surface silanol groups [23,44,49].

The present work aims at quantitatively describing the uptake of chloride and ISA by cement paste with high slag content, CEM III/C (according to EN 197–1 [47]). All experiments target the unaltered CEM III/C with a pH ≈ 13.1. A series of sorption experiments using radioactive $^{36}Cl^-$ were conducted in artificial pore solution containing NaCl concentrations up to 2.0 M. The evolution of cement mineralogy and pore solution composition was monitored and compared with thermodynamic calculations, in order to gain insight on the mechanisms driving the uptake of $^{36}Cl^-$. The uptake of ISA was investigated within 10^{-5} M < $[ISA]_0$ < 0.13 M, with the aim of quantifying the free ligand concentration remaining in solution in both cement systems, as well as assessing the impact of ISA in the pore solution composition, in particular with respect to Ca. The competition between chloride and ISA was also examined by means of sorption experiments at constant [ISA] and variable NaCl concentrations up to 2.0 M. The results obtained in this work for the binary and ternary systems CEM III/C-Cl^-, CEM III/C-ISA and CEM III/C-Cl^--ISA provide key inputs for the interpretation of the retention of radionuclides in the ternary and quaternary systems CEM III/C-Cl^--RN, CEM III/C-ISA-RN and CEM III/C-Cl^--ISA-RN, as exemplarily done within this project for niobium [17] and plutonium [45].

2. Materials and methods

2.1. Chemicals

All sample preparation and handling were conducted in Ar-glove boxes (MBRAUN) with O_2 < 1 ppm at T = (22 ± 2) °C. Purified water (Milli-Q, Millipore, 18.2 MΩ•cm) purged with Ar for several hours was used to prepare all aqueous solutions. NaOH, KOH (all Titrisol), Na_2SO_4, $Ca(OH)_2$, and NaCl (all EMSURE ®) were obtained from Merck. A carrier free $Na^{36}Cl$ in water was obtained from Eckert & Ziegler Analytic with a certified activity of 369 $kBq{\cdot}g^{-1}$. Isosaccharinic acid-1,4-lactone was obtained from Biosynth Carbosynth. Suprapur 65 % HNO_3 obtained from Merck was used for the dilution of samples for inductively coupled plasma atomic emission spectroscopy (ICP-OES) and liquid scintillation counting (LSC).

2.2. Preparation of cement paste and corresponding cementitious pore solution

The methods for all preparation, treatment, and characterization of cement paste and corresponding pore solution were described in [17]. Briefly, a CEM III/C 32.5 N-LH/SR CE LA BENOR cement clinker (provided by ONDRAF/NIRAS, Belgium) was mixed with Ar-purged Milli-Q water using a water-to-cement ratio of 0.46. The cement pastes were kept in closed moulds for setting for two days and then immersed in water for further curing during approximately 1.5 years. After curing, the surface layer (≈ 2.5 mm) was removed and the inner cement block was successively crushed, milled, and sieved. To avoid a size fractionation of different cement hydrates, the grinding was repeatedly performed until all cement power passed through a 63 μm sieve. A thorough characterization of the hydrated material by means of XRF and XRD (including Rietveld analysis) is given in Table 1, as reported in our previous work [17].

A second batch of CEM III/C-based pastes were prepared as described

Table 1
Composition of the CEM III/C cement used in this work. The elemental composition was determined by XRF, whereas the phase composition was determined by XRD with Rietveld analysis [17]. The slag content is determined by microscopic analysis.

	Chemical composition (g/100 g)		Phase composition (g/100 g)
SiO_2	32.31	Amorphous	88.4
Al_2O_3	9.33	Alite	5.9
Fe_2O_3	0.65	Belite	0.5
Cr_2O_3	< 0.003	Aluminate	0.5
MnO	0.222	Ferrite	0.4
TiO_2	0.636	Anhydrite	3.5
P_2O_5	0.08	Hemihydrate	0.3
CaO	45.28	Gypsum	0.2
MgO	7.27	Calcite	0.6
K_2O	0.52	Quartz	0.1
Na_2O	0.26	Gehlenite	0.2
SO_3	3.39		
Cl^-*	0.026		
Loss on ignition	0.17		
Total C	0.15		
Organic C	0.09		
Inorganic C	0.06		
CO_2	0.22		

previously and stored in closed polyethylene (PE) containers for 91 days. These pastes were used to determine the pore solution composition based on the squeezing method as described in [52,53]. The pore solution extracted from cement pastes was promptly filtered through a 0.45 μm nylon filter. The dissolved concentrations of Na, K, Ca, Si, and Al in the filtrate were analyzed by ICP-OES, and the concentrations of SO_4^{2-} and Cl^- were measured by ion chromatography (IC) as detailed in [17]. The pH of the extracted pore solution was measured by the electrode calibrated using standard solutions with known KOH concentrations [54]. The measured composition of squeezed pore solution was used to establish the recipe for artificial pore solution as described in [17]. An overall charge balance was taken into account for the definition of the recipe, whereas Ca concentration was slightly decreased to avoid the possible precipitation of portlandite (Table 2). Si and Al were excluded in the recipe due to their minor concentrations in the extracted pore solution ([Al] $< 10^{-4}$ M and [Si] $< 10^{-4}$ M). The artificial pore solution was prepared with NaOH and KOH solutions, Ar-purged purified water, Na_2SO_4, $Ca(OH)_2$, and NaCl.

2.3. Uptake of $^{36}Cl^-$ by CEM III/C

CEM III/C cement paste in the form of powder (particle size <63 μm) was equilibrated with natural Cl^- and active $^{36}Cl^-$ in the corresponding artificial cementitious pore solution (Table 2). Batch samples for Cl^- sorption experiments were prepared with solid-to-liquid ratios (S:L) = 5–100 g·L^{-1} and chloride concentrations ranging from $[Cl^-]_{PW}$ (intrinsic Cl^- concentration in the pore solution) = $3.2{\cdot}10^{-3}$ M to 2 M (adjusted by adding NaCl) in high-density polyethylene (HDPE) vials (Zinsser Analytic). A NaCl stock solution was prepared by dissolving the salt in artificial pore solution, and used for the spike of inactive Cl^- into the samples. The activity of $^{36}Cl^-$ in all sorption samples was set constant to 1 kBq, corresponding to $[^{36}Cl^-] = 1.16{\cdot}10^{-6}$ M. Batch samples were mechanically agitated, and sampled after contact times of 4, 65, and 79 days. Phase separation was achieved by 10 kDa ultrafiltration (Nanosep®, Pall Life Sciences, providing ca. 3 nm size cut-off), and the filtrate diluted in 2 vol% HNO_3 with a dilution factor of 2.5.

The uptake of $^{36}Cl^-$ was quantified by liquid scintillation counting (Tri-Carb 3110 TR, PerkinElmer) by adding the cocktail solution (Ultima Gold, PerkinElmer) into the diluted filtrate. The interference caused by ^{40}K present in the artificial pore solution was quantified as negligible, and the amount of $^{36}Cl^-$ sorbed on the vessel's wall and filter was minor (< 1 %). A separate batch sorption series was prepared following the same approach but using only natural NaCl, with the purpose of characterizing the cement paste and pore solution composition after equilibration with NaCl.

Solid phases were characterized by XRD using a Bruker D8 Advance X-Ray powder diffractometer with Cu Kα radiation at 2θ = 10–25°, incremental steps of 0.0082° and a measurement time of 1.5 s per step. The composition of the pore solution after 10 kDa ultrafiltration was analyzed by ICP-OES (Ca, Si, and Al) and IC (SO_4^{2-}). Distribution ratios (R_d) for $^{36}Cl^-$ sorption were calculated as described in Eq. (1).

Table 2
Summary of the artificial pore solution composition used in the present work for CEM III/C [17]. Uncertainty calculated as one standard deviation (σ) is provided in parentheses.

System	[Na] (mM)	[K] (mM)	[Ca] (mM)	[Cl^-] (mM)	[SO_4^{2-}] (mM)	pH
CEM III/C[a]	71 (± 1)	78 (± 1)	0.92[b] (± 0.16)	3.2 (± 0.1)	3.5 (± 0.9)	13.1 (± 0.1)

[a] Composition of squeezed pore solution (in mM): Na: 70, K: 77 Ca: 2.9; S: 3.62, Cl: 2.1, Al: 0.1, Si: 0.09, pH 13.0, as reported in [17].
[b] Ca concentrations in the artificial pore solution were decreased to avoid oversaturation with respect to portlandite.

$$R_d = \frac{\left[^{36}Cl^-\right]_{solid}}{\left[^{36}Cl^-\right]_{aq}} = \frac{A_0\left(^{36}Cl\right) - A_{aq}\left(^{36}Cl\right)}{A_{aq}\left(^{36}Cl\right)} \cdot \frac{V}{m} \quad (1)$$

where $\left[^{36}Cl^-\right]_{solid}$ is the concentration of $^{36}Cl^-$ sorbed on cement paste (mol·kg^{-1}), $\left[^{36}Cl^-\right]_{aq}$ is the concentration of $^{36}Cl^-$ in the aqueous phase (mol·L^{-1}), $A_0(^{36}Cl)$ is the initial activity of $^{36}Cl^-$ (1000 Bq) in aqueous phase (Bq), $A_{aq}(^{36}Cl)$ is the activity of $^{36}Cl^-$ in the aqueous phase after sorption (Bq), V is the volume of sample (L), and m is the mass of cement paste in sorption sample (kg).

2.4. Uptake of isosaccharinic acid by CEM III/C-based pastes

CEM III/C cement paste in the form of powder (particle size <63 μm) was equilibrated with ISA in corresponding artificial cementitious pore solution (Table 2). Batch samples for ISA sorption experiments were prepared with S:L = 2–50 g·L^{-1} and 10^{-5} M < [ISA] < 0.13 M in HDPE vials (Zinsser Analytic). A 1.49 M ISA stock solution was prepared by dissolving ISA lactone in 1 M NaOH + KOH solution and characterized by Nuclear Magnetic Resonance (NMR) showing the total conversion to the linear form of ISA [17]. The ISA stock solution was diluted in a mixture solution of 0.071 M NaOH and 0.078 M KOH and added into the sorption sample to obtain a desired concentration. After a contact time up to 49 days, phase separation was conducted with a syringe filtration of 0.45 μm (PTFE) and the filtrate was used to quantify ISA sorption using non-purgeable organic carbon (NPOC, Analytik Jena multi n/c 2100 S equipment) as detailed in [17]. An aliquot of the filtrate was characterized by ICP-OES (Ca, Si, and Al) and IC (SO_4^{2-}) subsequent to the dilution in 2 vol% HNO_3 and purified water, respectively.

Distribution ratios (R_d) for ISA sorption were calculated as described in Eq. (2)

$$R_d = \frac{[ISA]_{solid}}{[ISA]_{aq}} = \frac{[ISA]_0 - [ISA]_{aq}}{[ISA]_{aq}} \cdot \frac{V}{m} \quad (2)$$

where $[ISA]_{solid}$ is the concentration of ISA sorbed on cement paste (mol·kg^{-1}), $[ISA]_{aq}$ is the concentration of ISA remaining in aqueous phase (mol·L^{-1}), $[ISA]_0$ is the initial concentration of ISA in aqueous phase (mol·L^{-1}), V is the volume of sample (L), and m is the mass of cement paste in sorption sample (kg).

2.5. Calculation of saturation indices for NaCl system

Thermodynamic calculations of the saturation indices of cement hydrates were carried out with GEM-Selektor v3.9 [55,56], a Gibbs free energy minimization geochemical modeling program. Standard thermodynamic data for the species or components of aqueous, solid, and gas phases were taken from the PSI-Nagra thermodynamic database [57], while data for cement hydrates were taken from the Cemdata18 database [58]. The C-S-H was modeled using the quaternary solid solution model for C-S-H (CSHQ) [58,59].

The saturation index (SI) with respect to a solid are calculated from the tabulated solubility product (K_s) of the respective solid and from the ion activity product (IAP) obtained from activities derived from the total concentrations measured in the solution, i.e., SI = log(IAP/K_s). The saturation indices for relevant solid phases were calculated based on the experimentally measured total concentrations of ions and pH values. Activity coefficients were calculated using the extended Debye-Hückel equation in Truesdell-Jones form as described in Eq. (3):

$$log\gamma_i = \frac{-A_y z_i^2 \sqrt{I}}{1 + B_y a_i \sqrt{I}} + b_y I \quad (3)$$

where ionic strength (I in mol·kg$_w^{-1}$), Debye-Hückel constants (A_y in kg$^{1/}$

^{2}·mol$^{-1/2}$ and B_y in kg$^{1/2}$·mol$^{1/2}$·Å^{-1}), common ion-size parameter a_i = 3.67 Å for KOH solutions, and third parameter b_y = 0.123 kg·mol^{-1} [60]. This activity correction is applicable up to approximatively 1 mol·kg$_w^{-1}$ ionic strength [61]. The extended Debye-Hückel equation was preferred over a Pitzer model due to the lack of Pitzer parameters describing the specific interactions of Al—Si, Ca—Si and Al—K, as well as the incomplete availability of all SIT (Specific ion interaction theory) coefficients required for this system [62]. The saturation indices calculated at high salt concentration (i.e., 1 and 2 M NaCl) should thus be considered as approximate values.

A positive SI implies oversaturation and thus the possibility of precipitation of the respective phase, while a negative SI indicates undersaturation and (potential) dissolution of the respective solid. The use of saturation indices can be misleading if solids that dissociate into a different number of ions are compared. To improve comparability, "effective" saturation indices (ESI) were often used [9], obtained dividing the saturation indices by the number of ions participating in the reactions. i.e., the saturation indices for portlandite, C-S-H, ettringite, gypsum and Friedel's salt were divided by 3, 3, 15, 2 and 12, respectively, as detailed in [63].

3. Results and discussion

3.1. Uptake of $^{36}Cl^-$ by CEM III/C cement paste

No clear correlation of chloride uptake with contacting time (4, 65, and 79 days) was found in the kinetic series (see Fig. SI-1 in the Supporting Information). Sorption equilibrium was attained within 4 days, confirming the fast uptake of Cl^- as previously reported in the literature [23]. Hence, average distribution coefficients, R_d values, and corresponding uncertainties were obtained based on the measurements at three different contacting times.

The uptake of chloride by CEM III/C paste, (Fig. 1 and Table 3) expressed as R_d values, follows the same trend as reported for PC in previous sorption studies [23,26,49,64]. The R_d values obtained in this work (CEM III/C paste at pH ≈ 13.1, see Table 3) are comparable but slightly higher than those reported by Jain et al. (PC at pH ≈ 13.3) [26] and Jo et al. (PC at pH ≈ 13.5) (see Table 3) [23]. The higher sorption capacity of CEM III/C paste compared to PC [23,26] can be attributed to variations in both the assemblage of cementitious hydrates and the composition of pore solution. In the CEM III/C paste, comprising ~88 wt % of slag [17], in addition to C-S-H and AFm phases also hydrotalcite is present [65,66], which could contribute to an enhanced Cl^- uptake [18–21]. For the same CEM III/C paste, our previous study identified hydrotalcite (< 10 wt%) by means of thermogravimetric analysis and differential weight loss [17]. Differences in the sorption capacity are also likely related to the differences in the pore solution pH used in these studies (i.e., decreasing Cl^- binding with increasing pH [67]), and the corresponding implications in the surface properties of these materials. In particular, surface charge (measured in terms of zeta potentials) decreases from positive to negative values when increasing the pH from 12.5 to 13.3 [49,68], which expectedly results in a decreased sorption of

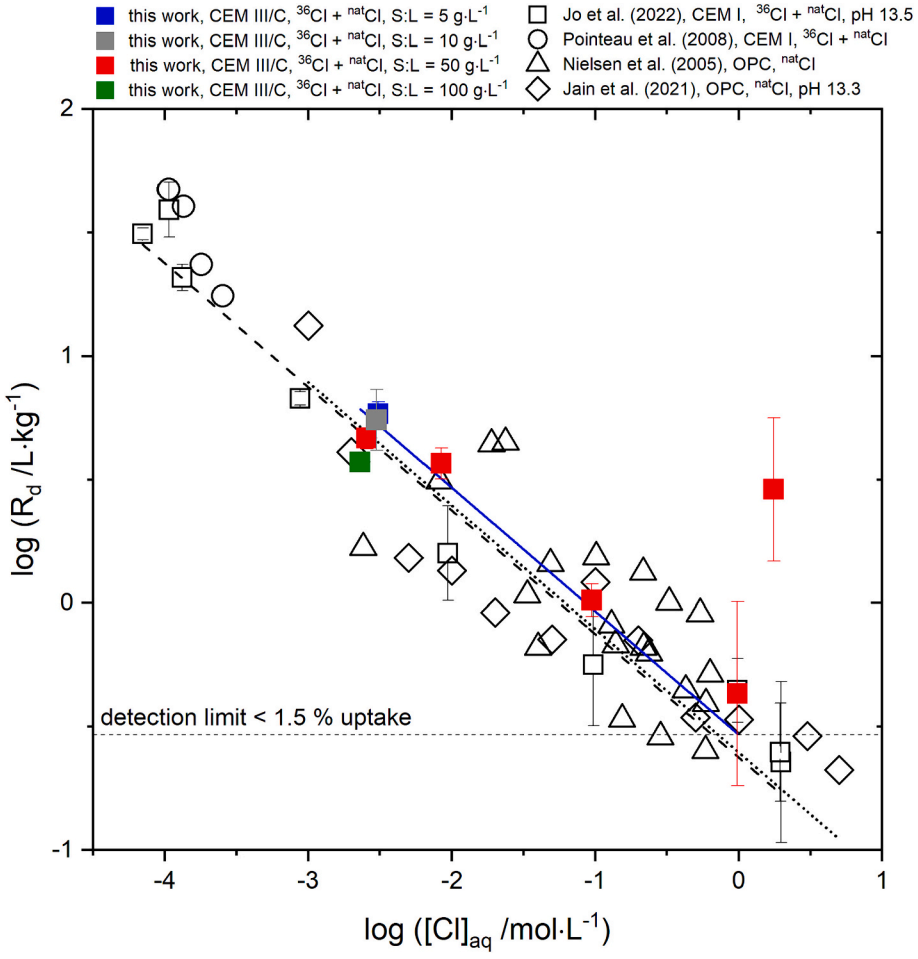

Fig. 1. Distribution ratios (R_d) of $^{36}Cl^-$ determined in this work using CEM III/C paste with $[Cl^-]_{PW}$ ($3.2{\cdot}10^{-3}$ M) < $[Cl^-]$ < 2.0 M and S:L = 5–100 g·L^{-1} (solid symbols) or reported in the literature (empty symbols) [23,26,49,64]. All sorption data determined at pH > 12.8. The slope of lines crossing the data are −0.5 (solid line: this work, dashed line: [23], and dotted line: [26]). The detection limit was defined as 1.5 % $^{36}Cl^-$ uptake, calculated as 3 times the standard deviation of reference solutions. All experimental data points are summarized in Table SI-1 of the Supporting Information.

Table 3
Summary of sorption data for chloride by type of cement considered in Fig. 1 (relevant to cement degradation stage I at pH > 12.8).

Cement type	[Cl] range/M	S:L ratio /g·L^{-1}	Contact solution	Equilibration time	R_d /L·kg^{-1}	Reference
CEM III/C	$1.1\cdot10^{-4}$–2.0 (^{nat}Cl) $1\cdot10^{-6}$ (^{36}Cl)	5–100	pH = 13.1, [Na] = 0.071 M, [K] = 0.078 M, [Ca] = $9.2\cdot10^{-4}$ M, $[Cl^-]_{PW} = 3.2\cdot10^{-3}$ M, $[SO_4^{2-}] = 3.5\cdot10^{-3}$ M	4–79 days	0.43–5.8	This work
CEM I	$1.1\cdot10^{-4}$–2.0 (^{nat}Cl) $1\cdot10^{-6}$ (^{36}Cl)	10–100	pH = 13.5, [Na] = 0.14 M, [K] = 0.37 M, [Ca] = $1.4\cdot10^{-3}$ M, $[Cl^-]_{PW} = (1.4–1.7)\cdot10^{-4}$ M, $[SO_4^{2-}] = 2\cdot10^{-3}$ M	44 days	0.25–37	[23]
White and grey (ordinary) Portland cement	0.01–1.0 (^{nat}Cl)	660	NaOH solution: [Na] = 0.25 and 0.55 M	6 months	0.3–5	[64]
CEM I	$(1–3)\cdot10^{-4}$ (^{nat}Cl) $7\cdot10^{-8}$ (^{36}Cl)	1–7	Cement contacting water containing K and Na: pH 12.8–13.3, [Ca] = $1.2–6.7\cdot10^{-3}$ M, $[Cl^-]_{PW} = (1.0–2.6)\cdot10^{-4}$ M, $[SO_4^{2-}] = (0.4–2.4)\cdot10^{-4}$ M	1 month	≈ 10	[49]
CEM I	10^{-3}–5 (^{nat}Cl)	–	Synthesized PW: pH 13.3, [Na] = 0.1 M, [K] = 0.19 M, [Ca] = 0.027 M	3 days	0.2–13	[26]

anionic species. A consistent effect of pH on the uptake of anionic radionuclides was clearly shown by Pointeau and co-workers for $^{125}I^-$, $^{14}CO_3^{2-}$, $^{75}SeO_3^{2-}$ and $^{36}Cl^-$ [49].

A systematic decrease in the R_d values was observed when increasing the chloride concentration up to [NaCl] ≤ 1 M (Fig. 1) indicating that a higher fraction of chloride remained in solution. At S:L = 50 g·L^{-1}, distribution ratios of $^{36}Cl^-$ in CEM III/C paste decreased from log R_d (in L·kg^{-1}) = (0.67 ± 0.04) at $[Cl^-]_{aq} = 2.6\cdot10^{-3}$ M to –(0.37 ± 0.37) at $[Cl^-]_{aq}$ = 1.0 M. As previously discussed in the literature, this observation supports that the uptake of Cl^- is mostly driven by the total chloride concentration in the aqueous phase, $[Cl^-]_{aq}$ [2,23]. At [NaCl] = 2.0 M NaCl, an unexpected increase in the uptake of $^{36}Cl^-$ is observed. The experiment was repeated four times, in each case involving the sampling of three replicates. All these measurements consistently showed an enhanced sorption, with log $R_d \approx 0.5$, which could be related to the formation of Friedel's salt.

Sorption by C-S-H and uptake by AFm via the formation of Friedel's salt were suggested as main sorption mechanisms in PC [2]. In the case of CEM III/C paste, where also hydrotalcite can play a more significant role in Cl^- uptake, the relative contribution of these sorption sinks, i.e., hydrotalcite, AFm, and C-S-H, at varying $[Cl^-]_{aq}$ remains unclear.

In our previous work [17], XRD and thermogravimetric analysis indicated the presence of mainly C-S-H and ettringite in the cement pastes, as well as the presence of some hydrotalcite (LDH) and monocarbonate for CEM III/C pastes, whilst portlandite was absent. The clear identification of the kind and amount of AFm in the CEM III/C paste is difficult due to its low fraction, poor crystallinity, and the overlap with the main signals of monocarbonate (at 2θ = 11.7°) and LDH (at 2θ = 11.6–11.7°) [69,70], which is in both cases related to the basal spacing. The basal spacing for both hydrotalcite as well as AFm phases such as Friedel's salt, monosulfate, hemicarbonate or monocarbonate varies with the interlayer anion and the amount of water [70,71], adding difficulties to the identification and quantification of the different LDH and AFm phases [70,71]. In fact, the formation of Friedel's salt is observed in 1 and 2 M NaCl solutions (see Fig. 2), but not at lower NaCl concentrations (0.1 M or lower) in agreement with other experimental observations in PC and blended cements, and with thermodynamic modeling predictions [72]. Two polymorphs of the Friedel's salt can be observed in hydrated cements depending on temperature and whether carbonate is present: rhombohedral, low-temperature Friedel's salt with a layer spacing of 7.9 Å exhibits a main signal at 2θ =11.2°, while above 37 °C the high-temperature monoclinic Friedel's salt with a layer spacing of 7.8 Å and main band at 2θ = 11.3° is stabilized [73]. The presence of carbonate stabilizes the monoclinic, high temperature polymorph of Friedel's salt at ambient temperature [74], with the interlayer distance varying as a function of the carbonate and chloride content [71,75]. In 1 and 2 M NaCl solutions, a relatively broad band at 2θ = 11.2–11.3° is observed, probably caused by the overlap of the signals of the two polymorphs.

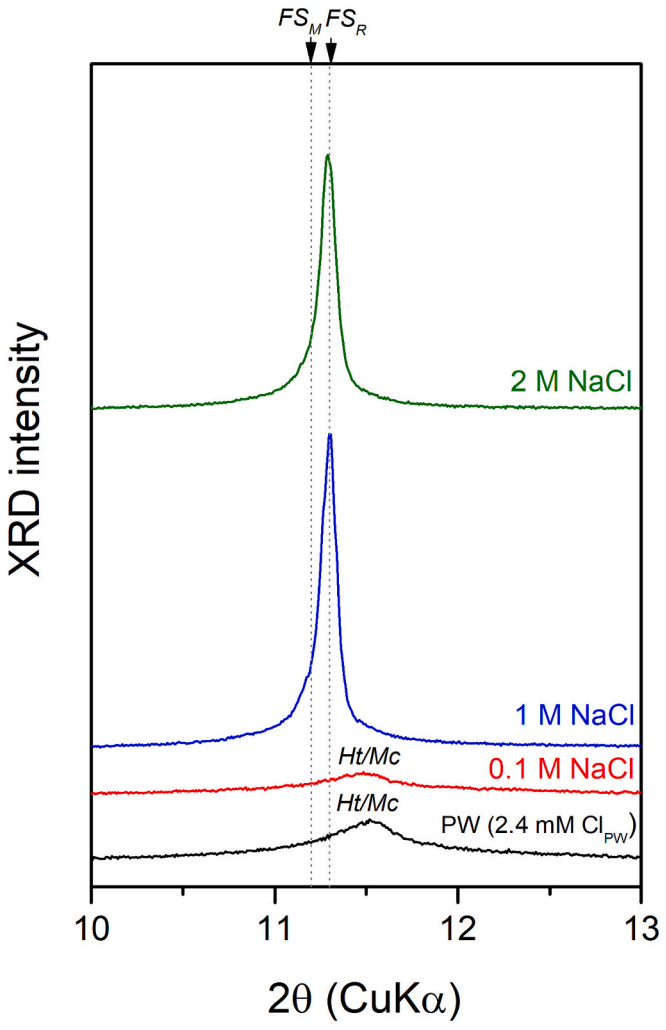

Fig. 2. X-ray diffraction patterns of dried CEM III/C pastes contacted with pore solution (S:L = 50 g·L^{-1}) containing $[Cl^-]_{PW}$ (intrinsic [Cl] without extra addition of NaCl) – 2 M NaCl. Contact time was >80 days for all samples. Ht/Mc: hydrotalcite and/or hemi- and monocarbonate, FS_R: rhombohedral Friedel's salt, and FS_M: monoclinic Friedel's salt.

Based on the comparison of the data obtained in this work and previous data available in the literature, the effect of S:L on R_d is minor. No clear differences were found between R_d values determined in the

experiments combining $^{36}Cl^{-}$ + $^{nat}Cl^{-}$ and those using only inactive $^{nat}Cl^{-}$ (Table 3 and Fig. 1), thus indicating that isotopic exchange does not play a predominant role. This is particularly evident for systems with high $[Cl^{-}]_{tot}$ in the aqueous phase, for which chloride content in pristine cement paste (quantified as ≈ 55 ppm in CEM III/C paste, ≈ $1.5{\cdot}10^{-3}$ mol·kg^{-1} [2]) represents only a minor fraction of the overall chloride inventory in the system. Note however that isotopic exchange as mechanism for the retention of $^{36}Cl^{-}$ may gain relevance in repository systems, where the much higher S:L ratios result in a significantly larger pool of $^{nat}Cl^{-}$ available for isotopic exchange with $^{36}Cl^{-}$.

The composition of the equilibrating solutions of the CEM III/C cement paste was investigated with varying NaCl concentrations up to 2 M (Fig. 3 and Table 4). Fig. 3 shows a clear increase of [Ca] with increasing NaCl concentration, which is possibly related to the uptake of Na^{+} on C-S-H with the corresponding substitution / release of Ca^{2+} ions [76–78]. The profile of [Si] was similar to [Ca], but the increase in [Si] was relatively minor as compared to [Ca] (see Fig. 3), indicating an incongruent dissolution of cement paste (assumed to be mainly C-S-H) in the presence of NaCl. The increase in sulfur concentration observed at high NaCl concentrations is attributed to the substitution of SO_4^{2-} by Cl^{-} in AFm [79]. The concentration of Al decreased to 1 and 2 M NaCl, which could be related to the precipitation of Friedel's salt.

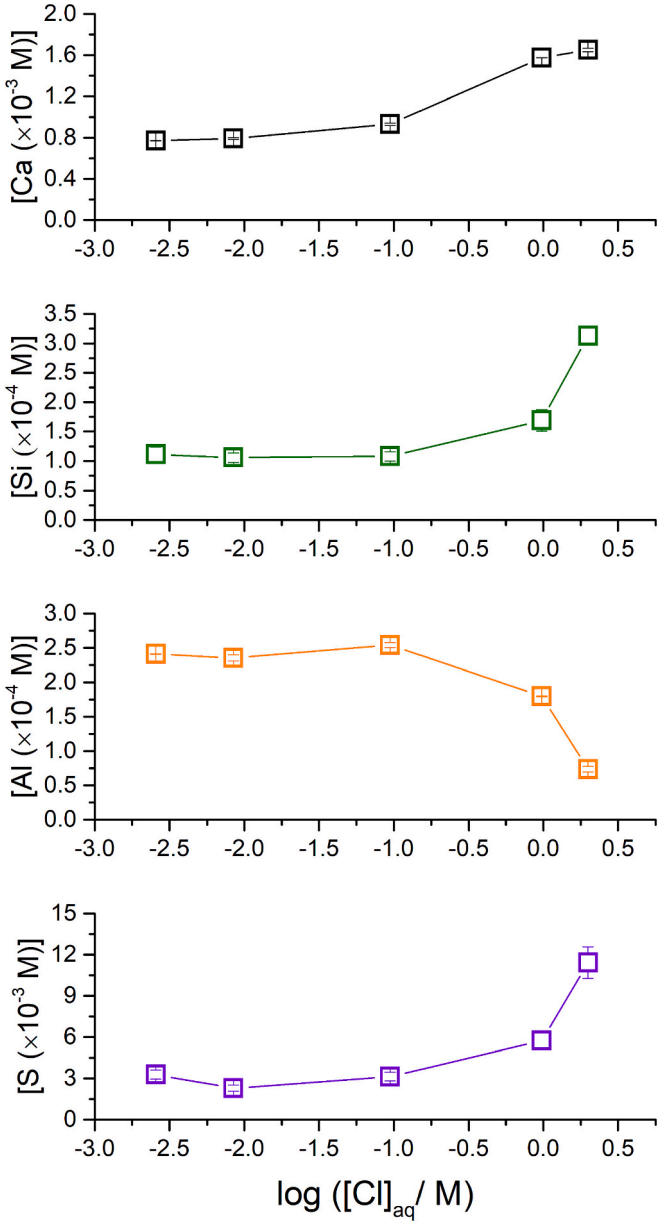

Fig. 3. Concentration of Ca, Si, Al, and S (measured by ICP-OES) in the pore solution of CEM III/C paste contacted with NaCl up to 2 M; contacting time > 80 days for all samples. Relative uncertainties are <10 % for the measured concentrations.

Table 4 summarizes the calculated effective saturation indices, SI, using the composition of the equilibrating solutions of CEM III/C paste with increasing NaCl concentrations. Calculations show that all solutions are saturated with respect to C-S-H and ettringite. Calculations for the equilibrating solutions at [NaCl] < 1 M indicate the undersaturation with respect to Friedel's salt, whereas oversaturation conditions are predicted for 1 and 2 M NaCl. These calculations are in excellent agreement with observations by XRD (Fig. 2).

3.2. Uptake of ISA by CEM III/C paste

Fig. 4 shows the data determined in this work for the uptake of ISA by CEM III/C paste, represented as log $[ISA]_{solid}$ vs. log $[ISA]_{aq}$. Sorption capacity observed in this work for CEM III/C paste is similar to that reported by Jo et al. [23] for CEM I-based materials in the degradation stage I (pH 13.5). However, they are slightly higher than the sorption capacities reported by Van Loon et al. [80] for CEM I in the degradation stage I (pH 13.4) and by Garcia et al. [51] for CEM V within the pH-range 12.5–13.3. Such deviations can be explained by differences in the particle size of the hardened paste used (i.e., < 63 μm in this work and in [23], 100–400 μm and < 200 μm in Van Loon et al. [80] and Garcia et al. [51], respectively), which affect surface area and thus the concentration of sorption sites per mass of cement paste. The figure includes also sorption data reported for C-S-H phases (Garcia et al. [51] and Missana et al. [44]), which show similar sorption capacities as those of cement pastes and thus underpins the main role of C-S-H in the uptake of ISA by hydrated cement systems. This observation does not preclude the possible contribution of other phases to the overall uptake of ISA, e.g., AFm or AFt phases with a remarkable affinity towards the retention of anions. Sorption data determined in this work are compared in Table 5 with other relevant studies investigating the uptake of ISA by hydrated cement in the degradation stages I and II.

The steep increase in log $[ISA]_{solid}$ observed at log $[ISA]_{aq} \geq -2$ is attributed to the precipitation of $Ca(ISA)_2$(cr). Although solubility calculations performed using thermodynamic data selected in the NEA-TDB [46] predict the precipitation of this solid phase at slightly higher ligand concentrations, log $[ISA]_{aq} \approx -1.2$, surface precipication can occur at lower concentrations than precipitation in bulk solution due to the higher concentrations achieved in the diffuse layer near the surface [81].

No clear impact of Na^{+} and Cl^{-} on the uptake of ISA by CEM III/C paste systems was observed up to 2 M NaCl (Fig. 5). This observation is consistent with the significantly higher distribution ratios determined in this work for the uptake of ISA (log $R_d \approx 1$ to 2.5) than for $^{36}Cl^{-}$ (log $R_d \approx -0.5$ to 0.8) by CEM III/C paste systems.

Sorption data for ISA obtained in this work were successfully modeled using a one-site Langmuir isotherm as described in Eq. (4).

$$[ISA]_{solid} = \frac{K \cdot q \cdot [ISA]_{aq}}{1 + K \cdot [ISA]_{aq}} \quad (4)$$

with K = (1057 ± 163) L·mol^{-1}; q = (0.29 ± 0.02) mol·kg^{-1}where $[ISA]_{solid}$ is the concentration of ISA sorbed on cement paste (mol·kg^{-1}), K is the adsorption affinity constant (L·mol^{-1}), q is the adsorption capacity (mol·kg^{-1}), and $[ISA]_{aq}$ is the concentration of ISA remaining in aqueous phase after sorption (mol·L^{-1}). We note that the model parameters determined in this work are in good agreement with K = (714 ± 266) L·mol^{-1} and q = (0.29 ± 0.04) mol·kg^{-1} of CEM I [23]. Van Loon et al. [80] used instead a two-site Langmuir isotherm to describe their

Table 4
Composition of the equilibrating solutions of CEM III/C paste with NaCl addition at S:L = 50 g·L^{-1} and contacting time > 80 days and the calculated effective saturation indices for portlandite, C-S-H, ettringite, gypsum, and Friedel's salt. Relative uncertainties <10 % for measured concentrations.

Cement type	NaCl addition	[Na] (mM)	[K] (mM)	[Ca] (mM)	[Mg] (mM)	[Cl][a] (mM)	[S] (mM)	[Si] (mM)	[Al] (mM)	pH[b]	effective saturation indices				
											portlandite	C-S-H	ettringite	gypsum	Friedel's salt
CEM III/C	No addition	72	74	0.72	< d.l.	2.56	3.3	0.1	0.2	13.12	– 0.2	0.0	0.1	– 1.2	– 0.4
	0.01	76	n.m.	0.79	< d.l.	8.43	2.3	0.1	0.2	n.m.	– 0.2	0.0	0.1	– 1.3	– 0.3
	0.1	166	n.m.	0.93	< d.l.	94.5	3.1	0.1	0.2	n.m.	– 0.2	0.0	0.1	– 1.3	– 0.1
	1	1030	n.m.	1.6	< d.l.	975	5.7	0.2	0.2	n.m.	– 0.2	0.1	0.0	– 1.3	0.0
	2	2000	n.m.	1.7	< d.l.	2000	11.4	0.3	0.07	n.m.	– 0.2	0.1	0.0	– 1.2	0.0

[a] Total chloride concentrations determined on the basis of ^{36}Cl measurements.
[b] Constant pH assumed for SI calculations. n.m. Not measured.

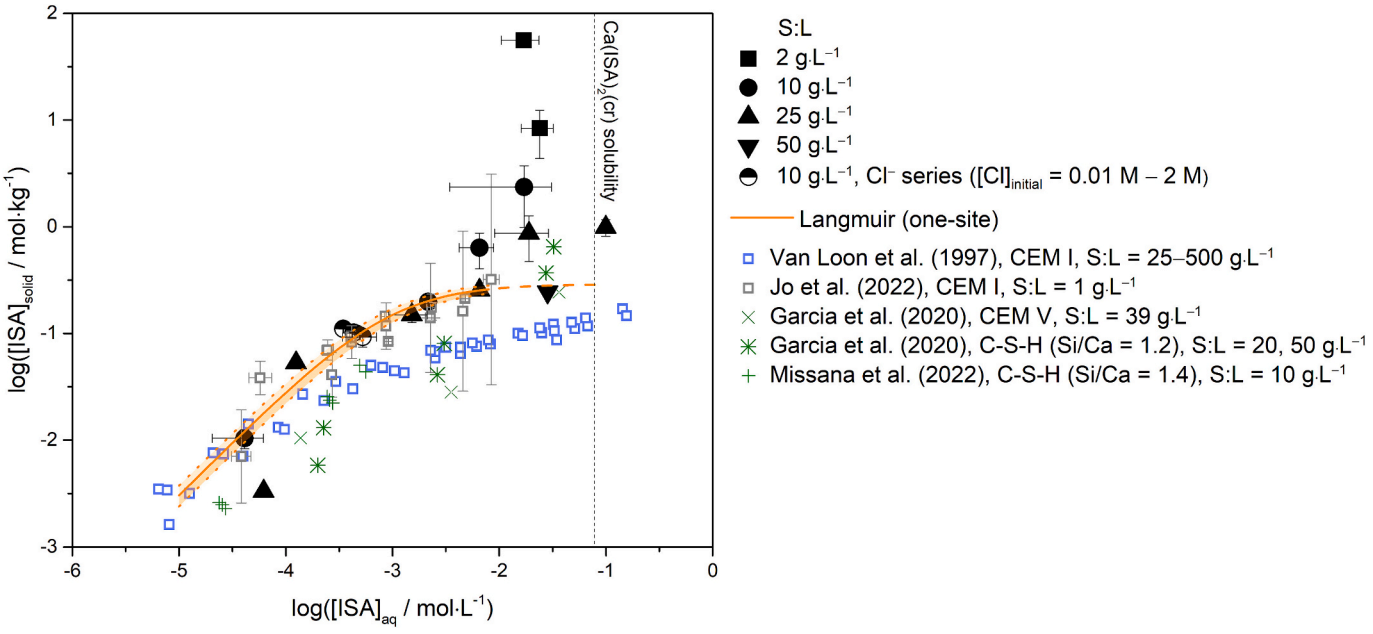

Fig. 4. Sorption isotherm of ISA on CEM III/C paste with initial [ISA] = 1.1·10^{-4}–1.3·10^{-1} M and S:L = 2–50 g·L^{-1} (solid symbol) and one-site Langmuir model (line and uncertainty area) with K = (1057 ± 163) L·mol^{-1} and q = (0.29 ± 0.02) mol·kg^{-1} derived in this work using the data at [ISA] < 10^{-2} M. Other sorption data reported in the literature [23,44,51,80] for cement systems at pH > 12 are plotted for comparison. The solubility line for $Ca(ISA)_2$(cr) was calculated for [Ca] = 4.8·10^{-3} M using thermodynamic data selected in the NEA-TDB [46]. This [Ca] was measured for CEM III/C paste pore solution with S:L = 2 g·L^{-1} (see Fig. 6).

sorption isotherm, with a second site emerging at [ISA] > 10^{-2} M. We note that the later study was conducted at pH = 13.4, for which the formation of $Ca(ISA)_2$(cr) is expected at higher ISA concentrations due to the formation of the ternary complex CaOHISA(aq) (alternatively formulated as $CaISA_{-H}$(aq), where ISA_{-H} corresponds to an ISA molecule with a deprotonated alcohol group). This enabled the authors to reach higher $[ISA]_{aq}$ than those obtained in this work, thus allowing an accurate definition of the two regions in the sorption isotherm. Pointeau et al. [49] derived a surface complexation model to explain their experimental data for the uptake of ISA as a function of pH. Two different sorption equilibria were proposed, including surface sites of C-S-H with and without Ca, i.e., >SOH and > $SOCa^+$, respectively). The model including the sorption sites >$SOCa^+$ was able to explain the experimental observations within the complete pH-range investigated, 11.7–13.3, whereas the model including only the sorption sites without Ca (>SOH) failed to reproduce the data at pH < 12.5. Missana et al. [44] also adopted the a surface complexation model approach to interpret their experimental data for the uptake of ISA by C-S-H phases with Ca:Si = 0.8 and 1.4. The model by Missana and co-workers also included the Ca-bearing sorption site (i.e., $SiOCa^+$), and was able to successfully explain experimental data showing a Langmuir-type trend at [ISA] < 10^{-3} M. Due to the low ISA concentrations used by the authors, the definition of only one sorption site was required. No clear improvement was achieved when including both weak and strong sites in the model. Recently, molecular dynamics (MD) calculations provided key insights for the mechanistic interpretation of ISA uptake by C-S-H phases [23]. MD calculations confirmed the relevant role of Ca as bridge between the C-S-H surface and ISA. This is in line with experimental findings available in the literature, which evidence the stronger sorption of anionic organic ligands (such as ISA and gluconate) by C-S-H with greater Ca:Si ratios [44,51,82].

The interaction of ISA with hydrated cement can also promote the dissolution of different cement phases, accordingly altering the mineralogy of the cement paste as well as the pore solution composition. Fig. 6 shows the evolution of Ca and Si concentrations as a function of $[ISA]_{aq}$. Both [Ca] and [Si] increase when increasing $[ISA]_{aq}$, although the increase is greater in the case of Ca. Due to the absence of portlandite in the investigated CEM III/C cement pastes (see [8]), this observation is explained by the incongruent dissolution of the C-S-H phases, which expectedly evolve towards lower Ca:Si ratios with increasing ISA concentrations.

At S:L = 2 g·L^{-1} and $[ISA]_{aq}$ = 0.1 M, 23 % of the total Ca inventory in the cement paste was leached out and stabilized as a Ca-ISA complex in the aqueous phase. This effect needs to be taken into account in the definition of sorption experiments with strongly sorbing radionuclides at low S:L ratios and high ISA concentrations.

Table 5
Summary of sorption data for ISA (relevant to cement degradation stages I and II at pH >12).

Cement type	Degradation stage / pH	log ([ligand]$_0$ / M)	S:L / g·L^{-1}	R_d / L·kg^{-1}	Particle size (μm)	Model and model parameters	Reference
CEM III/C	Stage I / 13.1	−3.8 to −0.9	2 − 50	9–900	< 63	Langmuir (one-site)[a] K = (1057 ± 163) L·mol^{-1} q = (0.29 ± 0.02) mol·kg^{-1}	This work
CEM I	Stage I / 13.5	−5 to −1	1	35–660	< 63	Langmuir (one-site) K = (714 ± 266) L·mol^{-1} q = (0.29 ± 0.04) mol·kg^{-1}	[23]
CEM I	Stage I / 13.4	–5 to −0.5	25–500	0.2–90	100–400	Langmuir (two-sites) K_1 = (1730 ± 385) L·mol^{-1} q_1 = (0.1 ± 0.01) mol·kg^{-1} K_2 = (12 ± 4) L·mol^{-1} q_2 = (0.17 ± 0.02) mol·kg^{-1}	[30,48,80]
CEM I	Stage II / 12.5	−3	0.2–50	64–100	< 100	Langmuir (two-sites) K_1 = (2510 ± 500) L·mol^{-1} q_1 = (0.18 ± 0.02) mol·kg^{-1} K_2 = (12 ± 2) L·mol^{-1} q_2 = (0.17 ± 0.02) mol·kg^{-1}	[42,50]
CEM V	Stage I / 13.3	−3.3 to −1.3	39	5–90	< 200	Langmuir (one-site, deviation at low [ISA])	[51]
	Stage II / 12.5	−3.3 to −1.3	39	15–730		Langmuir (one-site, deviation at low [ISA])	
C-S-H (Ca:Si = 1.2)	- / 12.1	−3.3 to −1.3	20 and 50	15–72	–	Langmuir(one-site)	
CEM I	Stage I / 12.8–13.3	−3.1	1	20–80	< 50	Surface complexation model	[49]
	Stage II / 12.5	−3.1	1	80			
C-S-H (Ca:Si = 1.4)	- /12.15	−4.3 to −3	10	80–110	–	Surface complexation model	[44]

[a] Parameters determined using the data points at $[ISA]_{aq} < 10^{-2}$.

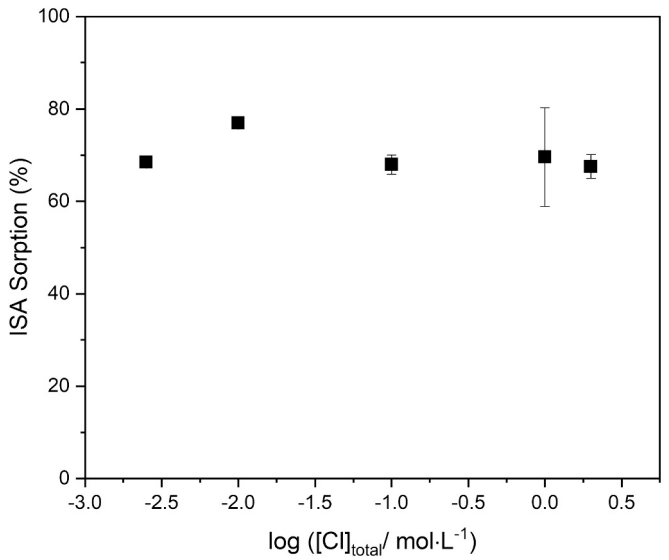

Fig. 5. Impact of chloride impact on the uptake of ISA by CEM III/C pastes (S:L = 10 g·L^{-1}, initial [ISA] = 1.4·10^{-3} M, [Cl$^-$] = 3.2·10^{-3} M – 2 M). The chloride was added in the form of NaCl.

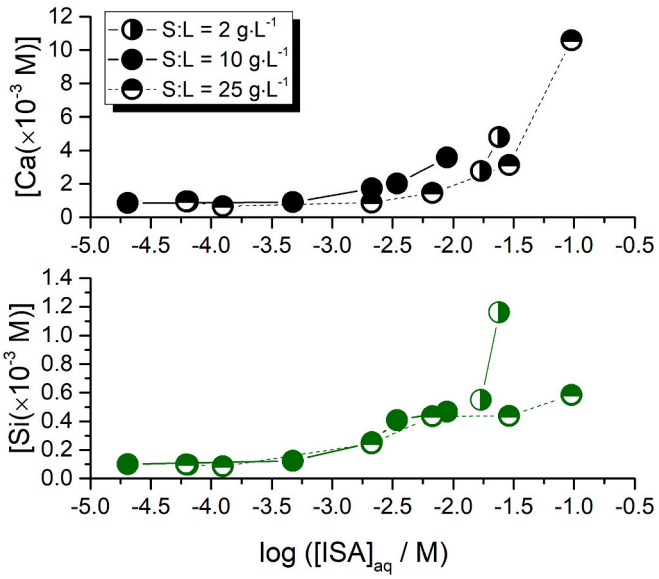

Fig. 6. Concentration of Ca and Si in the pore solution of CEM III/C paste (S:L = 2–25 g·L^{-1}) contacted with ISA (initial [ISA] = 1.1·10^{-4} M – 0.13 M).

4. Summary and conclusions

The retention of the anionic species Cl$^-$ and ISA by CEM III/C cement paste was investigated with a comprehensive series of sorption experiments covering the binary and ternary systems Cement-Cl$^-$, Cement-ISA and Cement-ISA-Cl$^-$. Sorption experiments were performed at pH ≈ 13.1, T = (22 ± 2) °C and under Ar atmosphere, with $[Cl^-]_{PW}$ (3.2·10^{-3} M) < $[Cl^-]_0$ < 2 M, 10^{-5} M < $[ISA]_0$ < 0.13 M and S:L = 2–100 g·L^{-1}. Sorption experiments with chloride were performed using a combination of $^{36}Cl^-$ and inactive $^{nat}Cl^-$.

The uptake of chloride by CEM III/C paste showed similar trends as reported in previous studies with CEM I, conducted both with $^{nat}Cl^-$ and $^{nat}Cl^- + {}^{36}Cl^-$. The slightly higher R_d values obtained in this work compared to previous studies are attributed to the effect of pH and the consequent impact on the surface charge of cement paste. Distribution ratios for the uptake of $^{36}Cl^-$ by CEM III/C paste gradually decrease from log R_d = (0.67 ± 0.04) L·kg^{-1} at $[Cl^-]_{aq}$ = 2.6·10^{-3} M to log R_d = (−0.37 ± 0.37) at $[Cl^-]_{aq}$ = 1.0 M, confirming that $[Cl^-]_{aq}$ is a key factor controlling the retention of $^{36}Cl^-$ of cement paste. In line with previous studies, C-S-H, AFm (as Friedel's salt) and hydrotalcite for CEM III/C cement paste are proposed as main sinks for the retention of Cl$^-$. XRD confirmed the formation of Friedel's salt in CEM III/C pastes contacted with 1 and 2 M NaCl, consistently with thermodynamic calculations using the Cemdata18 database. The concentration of Ca in the pore solution increased with increasing NaCl concentrations, as a result of the sorption of Na^+ on C-S-H with the consequent release of Ca^{2+} ions. The increase of sulfate concentration observed at high NaCl concentrations is induced by the substitution of SO_4^{2-} by Cl$^-$ in AFm.

A moderate sorption of ISA is confirmed for CEM III/C cement paste (with $R_d \approx 9$–900 L·kg^{-1}), in line with previous observations reported for CEM I and C-S-H phases. One-site Langmuir isotherm satisfactorily explains sorption data at $[ISA]_{aq} \leq 10^{-2}$ M, with $K = (1057 \pm 163)$ L·mol^{-1} and $q = (0.29 \pm 0.02)$ mol·kg^{-1}. The steep increase of $[ISA]_{solid}$ observed a $[ISA]_{aq} > 10^{-2}$ M is attributed to the (surface) precipitation of $Ca(ISA)_2$(cr). On the other hand, the interaction of ISA with hydrated cement promotes dissolution of cement phases with the non-stoichiometric increase of Ca and Si concentrations in the pore solution. Due to the absence of portlandite in the investigated CEM III/C cement pastes, this observation can be possibly explained by the incongruent dissolution of the C-S-H phases.

This study provides the basis for an accurate quantitative description of the retention of $^{36}Cl^-$ and ISA by CEM III/C cement pastes expected in some repository concepts for the disposal of L/ILW. The general uptake trends are similar to those observed for other cement formulations (e.g., CEM I). This study emphasizes the interplay between sorption and solubility phenomena in the Cement-ISA system, which needs to be taken into account for a correct prediction of the impact of ISA on the retention of radionuclides such as actinides or fission / activation products.

CRediT authorship contribution statement

Yongheum Jo: Writing – review & editing, Writing – original draft, Methodology, Investigation. **Barbara Lothenbach:** Writing – review & editing, Writing – original draft, Methodology, Investigation. **Neşe Çevirim-Papaioannou:** Methodology. **Benny de Blochouse:** Writing – review & editing, Project administration, Conceptualization. **Marcus Altmaier:** Writing – review & editing, Project administration, Funding acquisition, Conceptualization. **Xavier Gaona:** Writing – review & editing, Writing – original draft, Supervision, Project administration, Funding acquisition, Conceptualization.

Declaration of competing interest

The authors declare that they have no known competing financial interests or personal relationships that could have appeared to influence the work reported in this paper.

Data availability

Data will be made available on request.

Acknowledgements

This work was partly funded by ONDRAF/NIRAS. Darlyn Rehhorn, Frank Geyer, Annika Kaufmann, Sylvia Moisei-Rabung, Melanie Böttle, Jonas Rentmeister (all KIT–INE) and Luigi Brunetti (Empa) are gratefully acknowledged for the ICP-MS/OES, IC, LSC, NPOC measurements and technical support. Laura Caselles (ONDRAF/NIRAS) is kindly acknowledged for the thorough review of the manuscript.

Appendix A. Supplementary data

Supplementary data to this article can be found online at https://doi.org/10.1016/j.cemconres.2024.107509.

References

[1] M. Atkins, F.P. Glasser, Application of Portland cement-based materials to radioactive waste immobilization, Waste Manag. 12 (1992) 105–131.
[2] M. Ochs, D. Mallants, L. Wang, Radionuclide and Metal Sorption on Cement and Concrete, Springer, Switzerland, 2016.
[3] L. Duro, M. Altmaier, E. Holt, U. Mäder, F. Claret, B. Grambow, A. Idiart, A. Valls, V. Montoya, Contribution of the results of the CEBAMA project to decrease uncertainties in the safety case and performance assessment of radioactive waste repositories, Appl. Geochem. 112 (2020) 104479.
[4] E. Wieland, Sorption Data Base for the Cementitious near Field of L/ILW and ILW Repositories for Provisional Safety Analyses for SGT-E2, Nagra Technical Report 14–08, Paul Scherrer Institut, Villigen, Switzerland, 2014.
[5] I. Bonhoure, I. Baur, E. Wieland, C.A. Johnson, A.M. Scheidegger, Uptake of se(IV/VI) oxyanions by hardened cement paste and cement minerals: an X-ray absorption spectroscopy study, Cem. Concr. Res. 36 (2006) 91–98.
[6] B. Guo, K. Sasaki, T. Hirajima, Selenite and selenate uptaken in ettringite: immobilization mechanisms, coordination chemistry, and insights from structure, Cem. Concr. Res. 100 (2017) 166–175.
[7] L. Nedyalkova, J. Tits, G. Renaudin, E. Wieland, U. Mäder, B. Lothenbach, Mechanisms and thermodynamic modelling of iodide sorption on AFm phases, J. Colloid Interface Sci. 608 (2022) 683–691.
[8] S. Grangeon, N.C.M. Marty, N. Maubec, F. Warmont, F. Claret, Selenate sorption by hydrated calcium aluminate (AFm): evidence for sorption reversibility and implication for the modeling of anion retention, ACS Earth and Space Chemistry 4 (2020) 229–240.
[9] D. Jacques, Q.T. Phung, J. Perko, S.C. Seetharam, N. Maes, S. Liu, L. Yu, B. Rogiers, E. Laloy, Towards a scientific-based assessment of long-term durability and performance of cementitious materials for radioactive waste conditioning and disposal, J. Nucl. Mater. 557 (2021) 153201.
[10] J.L. García Calvo, A. Hidalgo, C. Alonso, L. Fernández Luco, Development of low-pH cementitious materials for HLRW repositories: resistance against ground waters aggression, Cem. Concr. Res. 40 (2010) 1290–1297.
[11] A. Vollpracht, B. Lothenbach, R. Snellings, J. Haufe, The pore solution of blended cements: a review, Mater. Struct. 49 (2016) 3341–3367.
[12] B. Lothenbach, K. Scrivener, R.D. Hooton, Supplementary cementitious materials, Cem. Concr. Res. 41 (2011) 1244–1256.
[13] L. Xinqi, H.W. Gäggeler, D. Laske, H. Synal, W. Wolfli, F.C.J. Brandt, J.C. Alder, K. Kurtz, Determination of the ^{36}Cl content in reactor cooling water and active resins from swiss nuclear power plants, Technical report 91–07, Wettingen, Switzerland, 1991.
[14] S.C. Sheppard, L.H. Johnson, B.W. Goodwin, J.C. Tait, D.M. Wuschke, C. C. Davison, Chlorine-36 in Nuclear Waste Disposal—1. Assessment Results for Used Fuel with Comparison to ^{129}I and ^{14}C, Waste Manage. (Oxford) vol. 16, 1996, pp. 607–614.
[15] S.J. Parry, B.A. Bennett, R. Benzing, D. Redpath, J. Harrison, P. Wood, F.J. Brown, Radiochemical neutron activation analysis for trace chlorine in steels and alloys, Anal. Chem. 69 (1997) 3049–3052.
[16] H.M. Sylla, F. Sybertz, Determination of the percentage of granulated blastfurnace slag in Portland slag cements and blastfurnace cements, ZKG Int. (1996) 108.
[17] Y. Jo, N. Çevirim-Papaioannou, K. Franke, M. Fuss, M. Pedersen, B. Lothenbach, B. de Blochouse, M. Altmaier, X. Gaona, Effect of ISA and Chloride on the uptake of niobium(V) by hardened cement paste and C-S-H phases: quantitative description and mechanistic understanding, Cem. Concr. Res. 172 (2023) 107233.
[18] O. Kayali, M.S.H. Khan, M. Sharfuddin Ahmed, The role of hydrotalcite in chloride binding and corrosion protection in concretes with ground granulated blast furnace slag, Cem. Concr. Compos. 34 (2012) 936–945.
[19] Y. Chen, Z. Shui, W. Chen, G. Chen, Chloride binding of synthetic ca–Al–NO3 LDHs in hardened cement paste, Construct. Build Mater. 93 (2015) 1051–1058.
[20] X. Ke, S.A. Bernal, J.L. Provis, Uptake of chloride and carbonate by mg-Al and ca-Al layered double hydroxides in simulated pore solutions of alkali-activated slag cement, Cem. Concr. Res. 100 (2017) 1–13.
[21] J. Zhang, C. Shi, Z. Zhang, Chloride binding of alkali-activated slag/fly ash cements, Construct. Build Mater. 226 (2019) 21–31.
[22] W. Wilson, J.N. Gonthier, F. Georget, K.L. Scrivener, Insights on chemical and physical chloride binding in blended cement pastes, Cem. Concr. Res. 156 (2022) 106747.
[23] Y. Jo, I. Androniuk, N. Çevirim-Papaioannou, B. de Blochouse, M. Altmaier, X. Gaona, Uptake of chloride and iso-saccharinic acid by cement: sorption and molecular dynamics studies on HCP (CEM I) and C-S-H phases, Cem. Concr. Res. 157 (2022) 106831.
[24] J. Tritthart, Chloride binding in cement II. The influence of the hydroxide concentration in the pore solution of hardened cement paste on chloride binding, Cem. Concr. Res. 19 (1989) 683–691.
[25] P. Hemstad, A. Machner, K. De Weerdt, The effect of artificial leaching with HCl on chloride binding in ordinary Portland cement paste, Cem. Concr. Res. 130 (2020) 105976.
[26] A. Jain, B. Gencturk, M. Pirbazari, M. Dawood, A. Belarbi, M.G. Sohail, R. Kahraman, Influence of pH on chloride binding isotherms for cement paste and its components, Cem. Concr. Res. 143 (2021) 106378.
[27] Y. Zhou, D. Hou, J. Jiang, L. Liu, W. She, J. Yu, Experimental and molecular dynamics studies on the transport and adsorption of chloride ions in the nano-pores of calcium silicate phase: the influence of calcium to silicate ratios, Microporous Mesoporous Mater. 255 (2018) 23–35.
[28] D. Hou, T. Li, P. Wang, Molecular dynamics study on the structure and dynamics of NaCl solution transport in the nanometer channel of CASH gel, ACS Sustain. Chem. Eng. 6 (2018) 9498–9509.
[29] I.-H. Svenum, I.G. Ringdalen, F.L. Bleken, J. Friis, D. Höche, O. Swang, Structure, hydration, and chloride ingress in C-S-H: insight from DFT calculations, Cem. Concr. Res. 129 (2020) 105965.
[30] L.R. Van Loon, M.A. Glaus, S. Stallone, A. Laube, Alkaline degradation of cellulose: estimation of the concentration of isosaccharinic acid in cement porewater, MRS Online Proc. Libr. 506 (1997) 1009–1010.
[31] M.A. Glaus, L.R. van Loon, S. Achatz, A. Chodura, K. Fischer, Degradation of cellulosic materials under the alkaline conditions of a cementitious repository for

low and intermediate level radioactive waste: part I: identification of degradation products, Anal. Chim. Acta 398 (1999) 111–122.
[32] M.A. Glaus, L.R. Van Loon, Degradation of cellulose under alkaline conditions: new insights from a 12 years degradation study, Environ. Sci. Technol. 42 (2008) 2906–2911.
[33] M. Ochs, F. Dolder, Y. Tachi, Decrease of radionuclide sorption in hydrated cement systems by organic ligands: comparative evaluation using experimental data and thermodynamic calculations for ISA/EDTA-actinide-cement systems, Appl. Geochem. 136 (2022) 105161.
[34] M. Keith-Roach, M. Lindgren, K. Källström, Assessment of Complexing Agent Concentrations in SFR, SKB, 2014.
[35] K. Vercammen, M.A. Glaus, L.R.V. Loon, Complexation of Th(IV) and Eu(III) by α-isosaccharinic acid under alkaline conditions, Radiochimica Acta 89 (2001) 393–402.
[36] X. Gaona, V. Montoya, E. Colas, M. Grive, L. Duro, Review of the complexation of tetravalent actinides by ISA and gluconate under alkaline to hyperalkaline conditions, J. Contam. Hydrol. 102 (2008) 217–227.
[37] D. Rai, A. Kitamura, Thermodynamic equilibrium constants for important isosaccharinate reactions: a review, J. Chem. Thermodyn. 114 (2017) 135–143.
[38] T. Kobayashi, T. Teshima, T. Sasaki, A. Kitamura, Thermodynamic model for Zr solubility in the presence of gluconic acid and isosaccharinic acid, J. Nucl. Sci. Technol. 54 (2017) 233–241.
[39] A. Tasi, X. Gaona, D. Fellhauer, M. Böttle, J. Rothe, K. Dardenne, R. Polly, M. Grivé, E. Colàs, J. Bruno, K. Källström, M. Altmaier, H. Geckeis, Thermodynamic description of the plutonium – α-d-isosaccharinic acid system I: solubility, complexation and redox behavior, Appl. Geochem. 98 (2018) 247–264.
[40] M.R. González-Siso, X. Gaona, L. Duro, M. Altmaier, J. Bruno, Thermodynamic model of Ni(II) solubility, hydrolysis and complex formation with ISA, Radiochimica Acta 106 (2018) 31–45.
[41] H.-K. Kim, H. Cho, K. Jeong, U.H. Yoon, H.-R. Cho, Thermodynamic study of am (III)–isosaccharinate complexation at various temperatures implicating a stepwise reduction in binding denticity, Inorg. Chem. 61 (2022) 19369–19378.
[42] A. Tasi, X. Gaona, T. Rabung, D. Fellhauer, J. Rothe, K. Dardenne, J. Lutzenkirchen, M. Grive, E. Colas, J. Bruno, K. Kallstrom, M. Altmaier, H. Geckeis, Plutonium retention in the isosaccharinate - cement system, Appl. Geochem. 126 (2021).
[43] N. Çevirim-Papaioannou, Y. Jo, K. Franke, M. Fuss, B. de Blochouse, M. Altmaier, X. Gaona, Uptake of niobium by cement systems relevant for nuclear waste disposal: Impact of ISA and chloride, Cem. Concr. Res. 153 (2022).
[44] T. Missana, M. García-Gutiérrez, U. Alonso, A.M. Fernández, Effects of the presence of isosaccharinate on nickel adsorption by calcium silicate hydrate (CSH) gels: experimental analysis and surface complexation modelling, J. Environ. Chem. Eng. 10 (2022) 108500.
[45] E. Coppens, K. Wouters, B. de Blochouse, D. Durce, Investigating the effect of pore water composition and isosaccharinic acid (ISA) on sorption of Pu to a CEM III/C-based mortar, Frontiers in Nuclear Engineering 2 (2023).
[46] W. Hummel, G. Anderegg, I. Puigdomènech, L. Rao, O. Tochiyama, Chemical thermodynamics Series Vol. 9: Chemical thermodynamics of compounds and complexes of U, Np, Pu, Am, Tc, Se, Ni And Zr with selected organic ligands, OECD Nuclear Energy Agency, 2005.
[47] E.N.19712011 CEN-CENELEC, Cement–Part 1: Composition, Specifications and Conformity Criteria for Common Cements, Brussels, Belgium, 2011.
[48] M.A. Glaus, A. Laube, L.R. Van Loon, Solid–liquid distribution of selected concrete admixtures in hardened cement pastes, Waste Manag. 26 (2006) 741–751.
[49] I. Pointeau, N. Coreau, P.E. Reiller, Uptake of anionic radionuclides onto degraded cement pastes and competing effect of organic ligands, Radiochim. Acta 96 (2008) 367–374.
[50] A.G. Tasi, Solubility, redox and sorption behavior of plutonium in the presence of α-D-isosaccharinic acid and cement under reducing conditions (Ph.D. Thesis), 2018.
[51] D. García, P. Henocq, O. Riba, M. López-García, B. Madé, J.-C. Robinet, Adsorption behaviour of isosaccharinic acid onto cementitious materials, Appl. Geochem. 118 (2020) 104625.
[52] P. Longuet, L. Burglen, A. Zelwer, La phase liquide du ciment hydraté, Revue des matériaux de construction 676 (1973) 35–41.
[53] B. Lothenbach, F. Winnefeld, Thermodynamic modelling of the hydration of Portland cement, Cem. Concr. Res. 36 (2006) 209–226.
[54] B. Traynor, H. Uvegi, E. Olivetti, B. Lothenbach, R.J. Myers, Methodology for pH measurement in high alkali cementitious systems, Cem. Concr. Res. 135 (2020) 106122.
[55] T. Wagner, D.A. Kulik, F.F. Hingerl, S.V. Dmytrieva, GEM-Selektor geochemical modeling package: revised algorithm and GEMS3K numerical kernel for coupled simulation codes, Can. Mineral. 50 (2012) 1173–1195.
[56] D.A. Kulik, T. Wagner, S.V. Dmytrieva, G. Kosakowski, F.F. Hingerl, K. V. Chudnenko, U.R. Berner, GEM-Selektor geochemical modeling package: revised algorithm and GEMS3K numerical kernel for coupled simulation codes, Comput. Geosci. 17 (2013) 1–24.
[57] T. Thoenen, W. Hummel, U. Berner, E. Curti, The PSI/Nagra Chemical Thermodynamic Data Base 12/07, PSI Report 14–04, Villigen, Switzerland, 2014.
[58] B. Lothenbach, D.A. Kulik, T. Matschei, M. Balonis, L. Baquerizo, B. Dilnesa, G. D. Miron, R.J. Myers, Cemdata18: a chemical thermodynamic database for hydrated Portland cements and alkali-activated materials, Cem. Concr. Res. 115 (2019) 472–506.
[59] D.A. Kulik, Improving the structural consistency of C-S-H solid solution thermodynamic models, Cem. Concr. Res. 41 (2011) 477–495.
[60] H.C. Helgeson, J.M. Delany, H.W. Nesbitt, D.K. Bird, Summary and critique of the thermodynamic properties of rock-forming minerals, Am. J. Sci. 278-A (1978) 229.
[61] B.J. Merkel, B. Planer-Friedrich, D.K. Nordstrom, Groundwater Geochemistry, A practical guide to modeling of natural and contaminated aquatic systems, Springer, Berlin, 2008.
[62] D.P. Prentice, S.A. Bernal, M. Bankhead, M. Hayes, J.L. Provis, Using the Pitzer model to predict aqueous solution compositions of Portland cements blended with supplementary cementitious materials, Proceedings of International Conferences (ICACMS) Advances in Construction Materials and systems 2 (2017) 638–647.
[63] B. Lothenbach, Thermodynamic equilibrium calculations in cementitious systems, Mater. Struct. 43 (2010) 1413–1433.
[64] E.P. Nielsen, D. Herfort, M.R. Geiker, Binding of chloride and alkalis in Portland cement systems, Cem. Concr. Res. 35 (2005) 117–123.
[65] S.-D. Wang, K.L. Scrivener, Hydration products of alkali activated slag cement, Cem. Concr. Res. 25 (1995) 561–571.
[66] A. Gruskovnjak, B. Lothenbach, L. Holzer, R. Figi, F. Winnefeld, Hydration of alkali-activated slag: comparison with ordinary Portland cement, Adv. Cem. Res. 18 (2006) 119–128.
[67] F. Avet, K. Scrivener, Influence of pH on the chloride binding capacity of limestone calcined clay cements (LC3), Cem. Concr. Res. 131 (2020) 106031.
[68] I. Pointeau, P. Reiller, N. Macé, C. Landesman, N. Coreau, Measurement and modeling of the surface potential evolution of hydrated cement pastes as a function of degradation, J. Colloid Interface Sci. 300 (2006) 33–44.
[69] M. Bellotto, B. Rebours, O. Clause, J. Lynch, D. Bazin, E. Elkaïm, A reexamination of Hydrotalcite crystal chemistry, J. Phys. Chem. 100 (1996) 8527–8534.
[70] E. Bernard, W.J. Zucha, B. Lothenbach, U. Mäder, Stability of hydrotalcite (mg-Al layered double hydroxide) in presence of different anions, Cem. Concr. Res. 152 (2022) 106674.
[71] F. Georget, B. Lothenbach, W. Wilson, F. Zunino, K.L. Scrivener, Stability of hemicarbonate under cement paste-like conditions, Cem. Concr. Res. 153 (2022) 106692.
[72] Z. Shi, M.R. Geiker, K. De Weerdt, T.A. Østnor, B. Lothenbach, F. Winnefeld, J. Skibsted, Role of calcium on chloride binding in hydrated Portland cement–metakaolin–limestone blends, Cem. Concr. Res. 95 (2017) 205–216.
[73] G. Renaudin, F. Kubel, J.P. Rivera, M. Francois, Structural phase transition and high temperature phase structure of Friedels salt, $3CaO \cdot Al_2O_3 \cdot CaCl_2 \cdot 10H_2O$, Cem. Concr. Res. 29 (1999) 1937–1942.
[74] A. Mesbah, J.-P. Rapin, M. François, C. Cau-dit-Coumes, F. Frizon, F. Leroux, G. Renaudin, Crystal structures and phase transition of cementitious bi-anionic AFm-(cl^-, CO_3^{2-}) compounds, J. Am. Ceram. Soc. 94 (2011) 261–268.
[75] A. Mesbah, C. Cau-dit-Coumes, F. Frizon, F. Leroux, J. Ravaux, G. Renaudin, A new investigation of the cl^-–CO_3^{2-} substitution in AFm phases, J. Am. Ceram. Soc. 94 (2011) 1901–1910.
[76] D. Sugiyama, Chemical alteration of calcium silicate hydrate (C–S–H) in sodium chloride solution, Cem. Concr. Res. 38 (2008) 1270–1275.
[77] G. Plusquellec, Analyse in situ de suspensions de silicate de calcium hydrat´e: Application aux interactions ioniques `a la surface des particules (Ph.D. thesis), Universite de Bougogne, Bourgogne, France, 2014.
[78] P. Henocq, A sorption model for alkalis in cement-based materials – correlations with solubility and electrokinetic properties, Physics and Chemistry of the Earth, Parts A/B/C 99 (2017) 184–193.
[79] M. Balonis, B. Lothenbach, G. Le Saout, F.P. Glasser, Impact of chloride on the mineralogy of hydrated Portland cement systems, Cem. Concr. Res. 40 (2010) 1009–1022.
[80] L.R. Van Loon, M.A. Glaus, S. Stallone, A. Laube, Sorption of isosaccharinic acid, a cellulose degradation product, on cement, Environ. Sci. Technol. 31 (1997) 1243–1245.
[81] K.P. Ananthapadmanabhan, P. Somasundaran, Surface precipitation of inorganics and surfactants and its role in adsorption and flotation, Colloids Surf. 13 (1985) 151–167.
[82] I. Androniuk, C. Landesman, P. Henocq, A.G. Kalinichev, Adsorption of gluconate and uranyl on C-S-H phases: combination of wet chemistry experiments and molecular dynamics simulations for the binary systems, Physics and Chemistry of the Earth, Parts A/B/C 99 (2017) 194–203.